

Calcium Carbonate–Gold Nanocluster Hybrid Spheres: Synthesis and Versatile Application in Immunoassays

Juan Peng,^[a] Li-Na Feng,^[a] Kui Zhang,^[b] Xing-Hua Li,^[a] Li-Ping Jiang,^{*[a]} and Jun-Jie Zhu^[a]

Abstract: Fluorescent gold nanoclusters (AuNCs) were incorporated into porous calcium carbonate spheres through electrostatic interaction. The resulting CaCO₃/AuNCs hybrid material exhibited interesting properties, such as porous structure, excellent biocompatibility, good water solubility, and degradability. These properties make the CaCO₃/AuNCs hybrid material a prom-

ising template to assemble horseradish peroxidase/antibody conjugates (HRP-Ab₂). By using CaCO₃/AuNCs/HRP-Ab₂ bioconjugates as probes, a versatile immunosensor was developed for fluo-

rescent and electrochemical detection of the cancer biomarker neuron-specific enolase (NSE). The detection limits of the sensor were 2.0 and 0.1 pg mL⁻¹ for fluorescent and electrochemical detection, respectively. The immunosensor shows high sensitivity and offers an alternative strategy for the detection of other proteins and DNA.

Keywords: calcium carbonate • electrochemistry • fluorescent probes • gold • immunoassays

Introduction

Gold nanoclusters (AuNCs) have attracted great attention in the past decade. Research interest ranges from fundamental properties such as photoluminescence,^[1–4] optical chirality,^[5–7] ferromagnetism,^[8] and quantized double-layer charging behavior^[9,10] to potential applications in optoelectronics,^[11] sensing,^[4,12–15] and bioassays.^[16–18] Compared to semiconductor quantum dots, which have larger size (3–100 nm) and contain toxic metal species (e.g., cadmium, lead), AuNCs are highly attractive because of their smaller size and nontoxicity.^[19] Moreover, AuNCs exhibit other fascinating features, including ease of synthesis, good water solubility, and surface functionalities, which also give them great promise in bioassays. However, direct bioconjugation of these AuNCs with biomolecules may induce aggregation during the cross-linking reaction, which influences the stability, precision, and reproducibility of the assay. Thus, a promising strategy is to use a porous template to encapsulate AuNCs.

Calcium carbonate (CaCO₃) is one of the main biomineral components of seashells. Polymorph control of CaCO₃ biomineral in seashells is achieved naturally by complex cellular cues. CaCO₃ has three different crystalline phases: vaterite, calcite, and aragonite. Porous CaCO₃ microspheres can be used as effective hosts for the fabrication of biocompatible hybrid materials due to their occurrence in nature as biominerals and their porous structure, which makes them suitable for the loading of other materials.^[20,21] Porous CaCO₃ microspheres have wide applications in drug delivery,^[22] biosensing,^[21,23–25] and protein encapsulation.^[20] The difficulty in using this attractive material for the design of multifunctional composites lies in its polymorphic character. The most attractive phase of CaCO₃ for the fabrication of multifunctional materials is the metastable vaterite form featuring spherical morphology and porous surface. Vaterite easily undergoes phase transition to the more thermodynamically stable phase of CaCO₃, calcite, which does not show the spherical, porous morphology of vaterite.^[20] This phase transformation usually occurs overnight for vaterite samples in water,^[20] which greatly limits their further application. CaCO₃ also shows good degradability, because it can be easily dissolved in ethylenediaminetetraacetic acid (EDTA) solution under mild conditions. Much research has been carried out on the fabrication and application of CaCO₃ microspheres with large size (larger than 3 μm).^[20,26] However, the large size limits their application in bioassay. Thus, a facile way of preparing CaCO₃ spheres of smaller size is highly required and of great challenge.

Hybrid materials with specific catalytic, magnetic, or optical properties have been fabricated.^[27–30] To the best of our knowledge, no report has been made on the fabrication of CaCO₃/AuNCs hybrid spheres. Due to the good biocompatibility of both CaCO₃ spheres and AuNCs, excellent fluores-

[a] J. Peng, L.-N. Feng, Dr. X.-H. Li, Dr. L.-P. Jiang, Prof. J.-J. Zhu
State Key Lab of Analytical Chemistry for Life Science
School of Chemistry and Chemical Engineering
Nanjing University, Nanjing, 210093 (P. R. China)
Fax: (+86)25-583-597-204
E-mail: Jianglp@nju.edu.cn

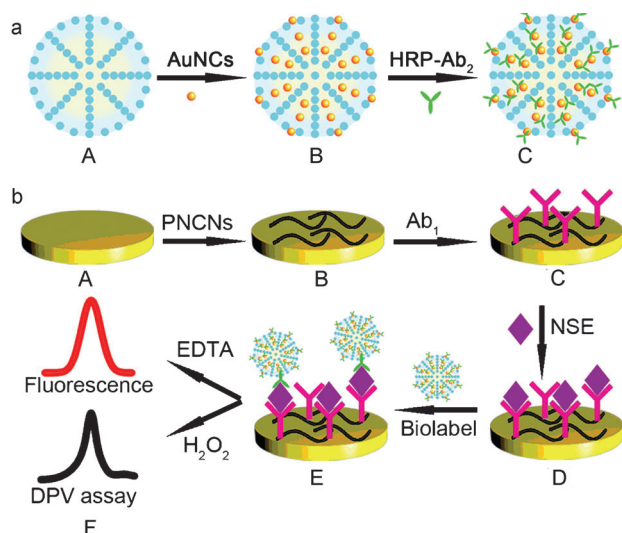
[b] Prof. K. Zhang
The Affiliated Drum Tower Hospital of
Nanjing University Medical School
Nanjing, 210008 (P. R. China)

Supporting information for this article is available on the WWW under <http://dx.doi.org/10.1002/chem.201102876>.

cent property of AuNCs, and porous structure of CaCO₃, CaCO₃/AuNCs hybrid material could find potential applications in drug delivery, bioassay, and biological systems.

Immunoassays based on specific molecular recognition of an antigen by its antibody have been widely used for quantitative analysis of protein biomarkers for clinical purposes. Numerous immunoassays have been developed for enhancement of detection sensitivity by signal amplification or employment of different detection technologies. Nanoparticle-based labeling systems have attracted special interest in immunoassays due to the outstanding optical, electronic, and biocompatible performance of nanoparticles.^[31,32] Here, CaCO₃/AuNCs hybrid spheres were employed to construct a labeling system for the fabrication of dual fluorescent and electrochemical detection platform.

In this work, a novel CaCO₃/AuNCs multifunctional material was synthesized and further used for the encapsulation of horseradish peroxidase/antibody conjugates (HRP-Ab₂) to fabricate CaCO₃/AuNCs/HRP-Ab₂ bioconjugates (Scheme 1). Fluorescent AuNCs were incorporated into



Scheme 1. a) Schematic illustration of fabrication process of CaCO₃/AuNCs/HRP-Ab₂ bioconjugate. A) Porous CaCO₃ sphere. B) CaCO₃/AuNCs hybrid sphere. C) CaCO₃/AuNCs/HRP-Ab₂ bioconjugate. b) Fabrication process of sandwich immunosensor for fluorescent and electrochemical detection of NSE. A) Glassy carbon electrode (GCE). B) PNCNs coated on GCE (GCE/PNCNs). C) Ab₁ immobilized on PNCNs surface (GCE/PNCNs/Ab₁). D) NSE targeted by immunoreaction. E) CaCO₃/AuNCs/HRP-Ab₂ captured by secondary immunoreaction. F) NSE detection by fluorescent and electrochemical DPV analysis.

CaCO₃ porous spheres. The resulting CaCO₃/AuNCs hybrid material retained the porous spherical structure, which provided an efficient template for the assembly of HRP-Ab₂ to construct a labeling system. The ability of CaCO₃/AuNCs/HRP-Ab₂ to act as probes was further examined by performing a sandwich bioaffinity immunoassay, as shown in Scheme 1b. Neuron specific enolase (NSE) is highly specific for neurons. Elevated NSE levels in serum can be attributed

to cerebral injury due to physical damage or ischemia caused by infarction or cerebral hemorrhage, coupled with increased permeability of the blood/brain barrier. The serum concentration of NSE has also been reported to correlate with the extent of damage and neurological outcome.^[33] Therefore, NSE was chosen as a protein model to evaluate the immunoassay. The coating antibody (Ab₁) was immobilized on polyethylenimine (PEI)-functionalized, nitrogen-doped multiwalled carbon nanotubes (PNCNs). Then, NSE was bound with Ab₁ through immunoreaction. Finally, CaCO₃/AuNCs/HRP-Ab₂ bioconjugates were captured during the specific binding event. The sensing signals could be detected by fluorescence and electrochemical differential pulse voltammetry (DPV).

Results and Discussion

Synthesis and characterization of the porous CaCO₃/AuNCs hybrid spheres: The porous CaCO₃ spheres were synthesized by a one-pot approach.^[34] Figure 1A shows TEM image of

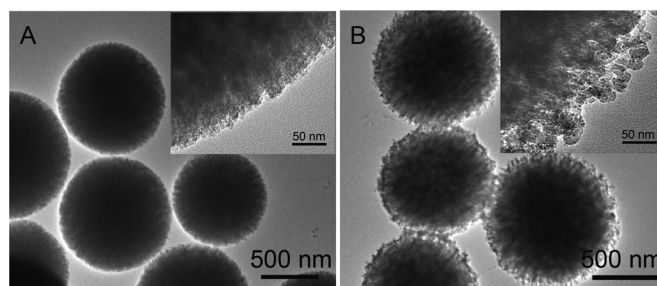


Figure 1. TEM images of A) CaCO₃ spheres. B) CaCO₃/AuNCs hybrid spheres. Insets: corresponding HRTEM images.

the CaCO₃ spheres, which have diameters in the range of 500–700 nm. A high-resolution TEM (HRTEM) image (inset in Figure 1A) showed that the CaCO₃ sphere has a unique structure and porous surface with pore size around 30 nm. The nanosized pores and channels in the CaCO₃ spheres provide efficient templates for encapsulation of bio-macromolecules such as enzymes and proteins through physical adsorption and pore diffusion.^[35] As shown in Figure S1 (Supporting Information), fluorescent AuNCs around 2 nm in size were synthesized and were well dispersed in deionized water. For the adsorption of AuNCs, poly(allylamine hydrochloride), PAH, was used to make the surfaces of the CaCO₃ spheres positively charged. Loading with AuNCs was carried out by dispersing the CaCO₃ spheres in an aqueous solution of AuNCs under sonication. Since the CaCO₃ spheres have positive surface charge (+16.5 mV) and AuNCs negative surface charge (−13.5 mV), the driving force for adsorption of AuNCs into the pores was mainly attributed to electrostatic interaction. Figure 1B shows TEM and HRTEM images of the CaCO₃/AuNCs hybrid spheres. The AuNCs incorporated into the CaCO₃ particles can be

clearly observed. The spherical and channel-like interior structure can also be observed in the HRTEM image (inset of Figure 1B). This result confirms that the AuNCs were successfully loaded into the CaCO_3 spheres.

The fabrication process was monitored by fluorescence spectroscopy. Figure 2A shows fluorescence spectra of the

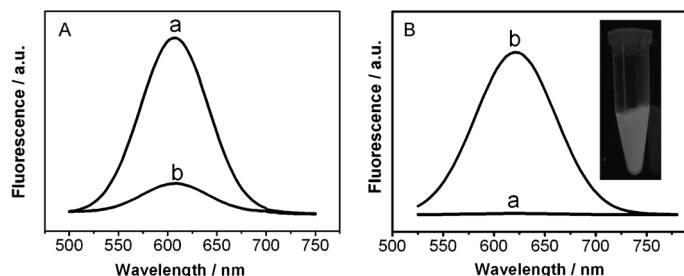


Figure 2. A) Fluorescence spectra of a) as-prepared AuNCs and b) the supernatant after AuNCs adsorption. B) Fluorescence spectra of a) CaCO_3 particles and b) CaCO_3 /AuNCs suspension. Inset of B) is a photograph of CaCO_3 /AuNCs aqueous solution under UV light.

as-prepared AuNCs solution (curve a) and the supernatant of the AuNCs solution after adsorption onto CaCO_3 particles (curve b). A great loss in fluorescence intensity was observed after loading of AuNCs, which indicates incorporation of the AuNCs into the CaCO_3 spheres. No fluorescence was observed for the CaCO_3 spheres (curve a in Figure 2B). In contrast, the CaCO_3 /AuNCs hybrid spheres showed strong fluorescence (curve b in Figure 2B), indicating effective loading of AuNCs, which are responsible for the strongly fluorescent property in the hybrid spheres. The loading amount of AuNCs in the CaCO_3 particles could be calculated by the difference in peak intensity of AuNCs solution before and after loading (Figure 2A). According to the concentration difference before adsorption ($344 \mu\text{g mL}^{-1}$) and after adsorption ($56 \mu\text{g mL}^{-1}$), a rough estimate indicated that 1.0 mg of CaCO_3 particles could accommodate 288 μg AuNCs.^[36,37] Confocal laser-scanning fluorescence microscopy was also employed to demonstrate the distribution of the AuNCs in the CaCO_3 spheres (Figure 3). This showed that the AuNCs could penetrate into the inner pores of CaCO_3 . The porous structure and open channels in the CaCO_3 spheres offer suitable microenvironments for AuNCs adsorption, and resulted in a large loading amount of AuNCs.

Because of the porous structure, the CaCO_3 spheres have a high surface area of $27.21 \text{ m}^2 \text{ g}^{-1}$ and pore volume of $0.1227 \text{ cm}^3 \text{ g}^{-1}$ (curve a in Figure S2, Supporting Information). After incorporation of AuNCs, the CaCO_3 /AuNCs hybrid spheres had a surface area of $20.60 \text{ m}^2 \text{ g}^{-1}$ and a pore volume of $0.0926 \text{ cm}^3 \text{ g}^{-1}$ (curve b in Figure S2, Supporting Information), which are smaller than those of the CaCO_3 spheres. In addition, a narrower pore-size distribution (inset of Figure S2, Supporting Information) and a sharp decrease in the number of large pores were observed, which might be attributed to infiltration of the AuNCs into the CaCO_3 particles. SEM images of both the CaCO_3 spheres and the

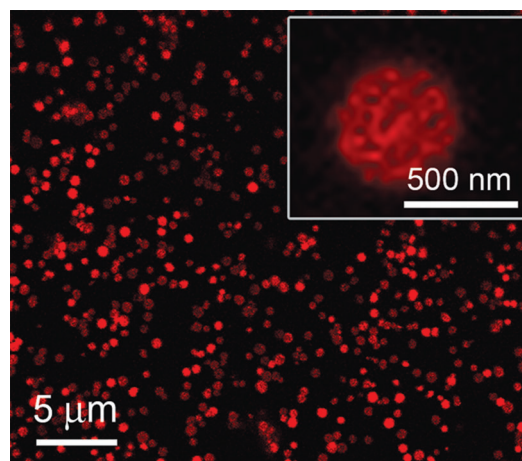


Figure 3. Confocal laser-scanning fluorescence image of CaCO_3 /AuNCs spheres. Inset: high-magnification confocal image of a CaCO_3 /AuNCs sphere.

CaCO_3 /AuNCs hybrid spheres are shown in Figure 4. As can be seen in Figure 4A, the surface of the CaCO_3 particles is porous and consists of numerous carbonate nanoparticles that form the specific morphology. This unique structure played an important role in the assembly of AuNCs. After incorporation of AuNCs, the surface became smooth (Figure 4B). It was found that loading with AuNCs could enhance the stability of CaCO_3 spheres consisting of the vaterite polymorph. When the CaCO_3 particles were stored in water for five days (Figure 4C), calcite began to form. In contrast, the CaCO_3 /AuNCs hybrid particles were stable as the vaterite polymorph in water for more than two months (Figure 4D). This result is confirmed by the XRD data in Figure S3 (Supporting Information). It is speculated that for-

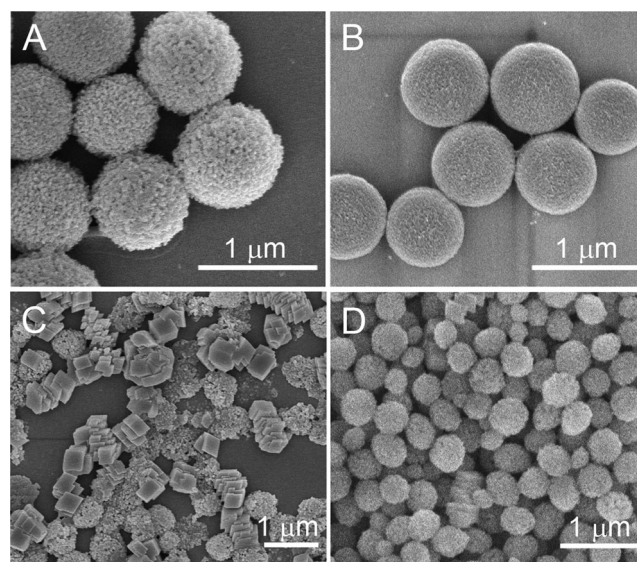


Figure 4. SEM images of A) vaterite CaCO_3 spheres, B) CaCO_3 /AuNCs hybrid spheres, C) calcite CaCO_3 acquired after five days, and D) CaCO_3 /AuNCs spheres after two months.

mation of thermodynamically stable compounds between the stabilizer and CaCO_3 is the main reason for the good stability of the hybrid. It is reported that a solid solution is formed between calcite carbonate and inorganic materials on the vaterite surface.^[38] These solid solutions show a lower heat of formation than calcite, and thus prevent dissolution of the vaterite polymorph. For comparison, gold nanoparticles (AuNPs) with a size of 20 nm were used to fabricate $\text{CaCO}_3/\text{AuNPs}$ hybrid spheres. The SEM image of the $\text{CaCO}_3/\text{AuNPs}$ hybrid spheres (Figure S4, Supporting Information) indicated that the calcite polymorph of CaCO_3 could easily form after one week. AuNPs of larger size less readily penetrate into the inner pores of CaCO_3 than AuNCs of smaller size, and hence the loading of AuNPs in CaCO_3 is greatly reduced. Thus, incorporation of AuNCs can efficiently stabilize the vaterite polymorph of CaCO_3 .

Assembly of protein on $\text{CaCO}_3/\text{AuNCs}$ hybrid spheres for biolabeling system: The $\text{CaCO}_3/\text{AuNCs}$ hybrid spheres inherited advantages from their parent materials, such as satisfactory biocompatibility, good solubility in water, and porous structure. Thus, the $\text{CaCO}_3/\text{AuNCs}$ hybrid spheres could be expected to be promising templates for protein loading. Then HRP- Ab_2 were encapsulated into the hybrid spheres and the obtained bioconjugates were used as versatile probes for immunoassay. Since the pI of HRP is 8.8,^[39] HRP- Ab_2 is positively charged at pH 7.0, and thus could be easily adsorbed on the hybrid spheres through electrostatic adsorption and interactions between AuNCs and the amino groups of the protein. Compared to $\text{CaCO}_3/\text{AuNCs}$ hybrid spheres, a smaller BET surface area ($13.62 \text{ m}^2 \text{ g}^{-1}$) and lower pore volume ($0.0682 \text{ cm}^3 \text{ g}^{-1}$) for $\text{CaCO}_3/\text{AuNCs}/\text{HRP-Ab}_2$ indicated effective loading of HRP- Ab_2 . Because of their small size, HRP- Ab_2 could penetrate into the pores, resulting in a decrease in the pore volume. Calculating the difference in enzyme concentration before and after adsorption revealed that about $180 \mu\text{g}$ of HRP- Ab_2 was captured by 1.0 mg of $\text{CaCO}_3/\text{AuNCs}$ hybrid spheres from a protein solution with a concentration of 0.4 mg mL^{-1} HRP- Ab_2 . When the hybrid material was conjugated with HRP- Ab_2 and kept in water for one month, vaterite was still the dominant polymorph. To demonstrate the potential application of $\text{CaCO}_3/\text{AuNCs}/\text{HRP-Ab}_2$ bioconjugates in bioassay, a sandwich immunoassay was developed.

Fabrication of a sandwich immunosensor by using $\text{CaCO}_3/\text{AuNCs}/\text{HRP-Ab}_2$ as probes: The utility of $\text{CaCO}_3/\text{AuNCs}/\text{HRP-Ab}_2$ bioconjugates for immunoassay was examined by using a model sandwich immunoassay for detection of NSE. Nitrogen-doped multiwalled carbon nanotubes (NCNs) have attracted considerable interest for constructing electrochemical biosensors because of their high electrical conductivity and excellent electrocatalytic effects.^[40] To fabricate the immunosensing surface, NCNs were used for immobilization of Ab_1 . To increase their solubility and biocompatibility, NCNs were initially acid-oxidized to introduce carboxyl groups on their surface (see Supporting Information for experimental

details), followed by the functionalization with polyethylenimine (PNCNs). Then, by employing glutaraldehyde as cross-linking agent, Ab_1 molecules could be firmly absorbed onto the PNCN surface through the interaction between amino-functionalized PNCNs and primary amino groups of the protein. As shown in Figure S5 (Supporting Information), SEM was employed to characterize the NCNs, PNCNs, and the Ab_1 immobilized on PNCNs (PNCNs/Ab_1). The NCNs showed a well-dispersed one-dimensional structure with diameter in the range of 20–40 nm. For PNCNs, no obvious change was observed in the morphology after PEI functionalization. When Ab_1 was immobilized on the surface, the thickness of PNCNs/Ab_1 clearly increased, which indicated that Ab_1 was effectively bound to the PNCN surface. The immunoassay process is outlined in Scheme 1b. First, Ab_1 was immobilized on the PNCN surface, and then NSE was bound with Ab_1 through the first immunoreaction. Subsequently, $\text{CaCO}_3/\text{AuNCs}/\text{HRP-Ab}_2$ bioconjugates were captured on the surface by the second immunoreaction. Finally, two applications were demonstrated to detect the target NSE concentration by using fluorescent and electrochemical DPV analysis. The details of the procedure are described in the Experimental section.

Fluorescence immunoassay: To be useful as a fluorescence biolabel, it is important that the loaded AuNCs can be released from the particles for fluorescence detection. In our work, AuNCs can be released from the captured $\text{CaCO}_3/\text{AuNCs}/\text{HRP-Ab}_2$ bioconjugates by dissolution of CaCO_3 templates in aqueous EDTA solution. Thus, the fluorescence of the AuNCs released from the biolabels was detected to determine the NSE concentration. The fluorescence intensity was strongly affected by the assay conditions (Figure S6, Supporting Information). After the Ab_1 concentration increased to $50 \mu\text{g mL}^{-1}$, the fluorescence intensity increased and tended to a stable signal at $30 \mu\text{g mL}^{-1}$. Thus, an Ab_1 concentration of $30 \mu\text{g mL}^{-1}$ was selected for the further studies. The fluorescence intensity increased with the incubation time between 10 and 30 min and then leveled off above 30 min. This result indicated that the interaction between antigen and antibody had reached equilibrium after 30 min, and hence an incubation time of 30 min was selected. The fluorescence response increased with increasing concentration and reached a platform at $50 \mu\text{g mL}^{-1}$ of the bioconjugates. Under optimal assay conditions, the fluorescence intensity with $\text{CaCO}_3/\text{AuNCs}/\text{HRP-Ab}_2$ probes (curve b in Figure 5A) was 8.54 times the signal when using AuNCs/HRP- Ab_2 probes (curve a in Figure 5A). This amplification of the fluorescence signal can mainly be attributed to the high loading amount of AuNCs on CaCO_3 spheres. As shown in Figure 5B and C, the fluorescence response of the immunosensor with $\text{CaCO}_3/\text{AuNCs}/\text{HRP-Ab}_2$ probes increased linearly with increasing logarithm of the target NSE concentration in the range from 0.005 to 1.0 ng mL^{-1} . The linear regression equation is $F/a.u. = 428.8 + 174.8 \lg(C_{\text{NSE}}/\text{ng mL}^{-1})$ with a linear regression coefficient of 0.995. The detection limit ($S/N=3$) is estimated to be 2.0 pg mL^{-1} .

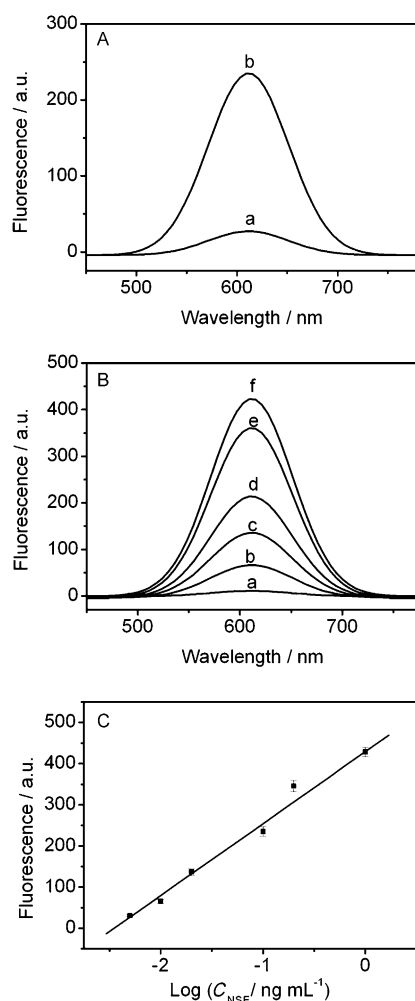
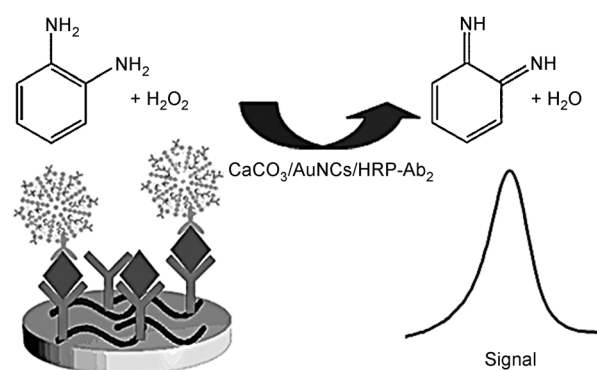


Figure 5. A) Fluorescence immunoassay in the presence of 0.1 ng mL^{-1} NSE. a) With AuNC/HRP- Ab_2 bioconjugates. b) With $\text{CaCO}_3/\text{AuNCs}/\text{HRP-Ab}_2$ bioconjugates. B) Fluorescence immunoassay with $\text{CaCO}_3/\text{AuNCs}/\text{HRP-Ab}_2$ bioconjugates at target NSE concentrations of 0.005, 0.01, 0.02, 0.1, 0.2, and 1.0 ng mL^{-1} (curves a–g, respectively). C) Linear relationship between fluorescence intensity and the logarithm of the target NSE concentration.

DPV analysis: The target NSE concentration was also detected electrochemically. It is well known that HRP can catalyze the oxidation of *o*-phenylenediamine (OPD) by H_2O_2 , and the mechanism of enzymatic catalysis and oxidation was investigated previously.^[41] The DPV response can be tested in 0.1 M pH 7.0 phosphate-buffered saline (PBS) containing OPD and H_2O_2 . The mechanism of the electrochemical oxidation of OPD is illustrated in Scheme 2. Multiple HRP in $\text{CaCO}_3/\text{AuNCs}/\text{HRP-Ab}_2$ bioconjugates can catalyze the oxidation of OPD with H_2O_2 . Figure 6A shows typical DPV curves for AuNCs-HRP- Ab_2 and $\text{CaCO}_3/\text{AuNCs}/\text{HRP-Ab}_2$ bioconjugates. A well-defined peak was observed around -0.521 V (vs. SCE) for the electrochemical oxidation of OPD to 2,2'-diaminoazobenzene, the enzymatic product.^[42] The DPV response was strongly influenced by the assay conditions. Therefore, the concentration of Ab_1 , incubation time, and concentration of bioconjugates were investigated



Scheme 2. Oxidation of OPD by H_2O_2 .

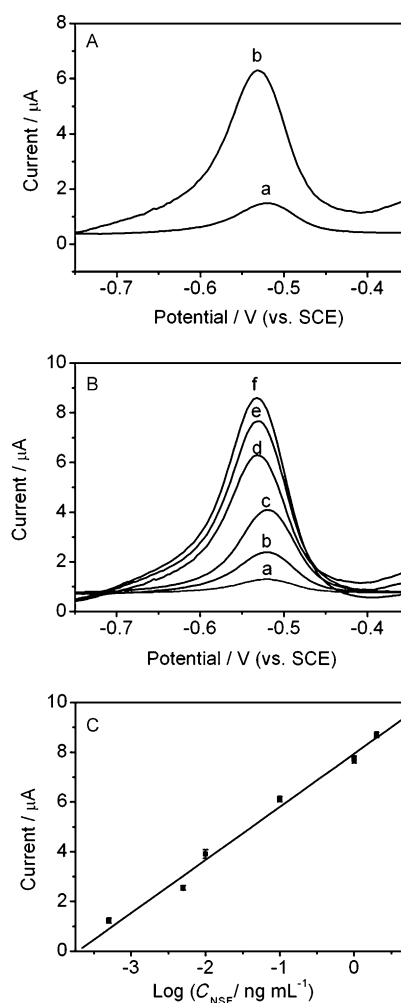


Figure 6. A) Electrochemical immunoassay in the presence of 0.1 ng mL^{-1} NSE. a) With AuNC/HRP- Ab_2 bioconjugates. b) With $\text{CaCO}_3/\text{AuNCs}/\text{HRP-Ab}_2$ bioconjugates. B) Typical DPV curves at target NSE concentrations of 0.0005, 0.005, 0.01, 0.1, 1.0, and 2.0 ng mL^{-1} (curves a–g, respectively). C) Linear relationship between current and the logarithm of the target NSE concentration.

(Figure S7, Supporting Information). An Ab_1 concentration of $30 \text{ } \mu\text{g mL}^{-1}$, an incubation time of 30 min, and a bioconjugate concentration of $50 \text{ } \mu\text{g mL}^{-1}$ were selected as optimal

assay conditions. The DPV signal with $\text{CaCO}_3/\text{AuNCs}/\text{HRP-Ab}_2$ probes (curve b in Figure 6A) was 4.24 times that with $\text{AuNCs}/\text{HRP-Ab}_2$ probes (curve a in Figure 6A). This also confirms that the signal was amplified by the high loading amount of $\text{AuNCs}/\text{HRP-Ab}_2$ on porous CaCO_3 . Figure 6B shows typical DPV curves of the immunoassay at different NSE concentrations under optimal conditions. The voltammetric peaks were well defined and the intensity was proportional to the concentration of NSE in the range from 0.0005 to 2.0 ng mL^{-1} . The resulting calibration plots were linear (Figure 6C). The linear regression equation is $I/\mu\text{A} = 7.944 + 2.138 \lg(C_{\text{NSE}}/\text{ng mL}^{-1})$ with a linear regression coefficient of 0.993. The detection limit ($S/N=3$) is estimated to be 0.1 pg mL^{-1} .

Compared to other reported electrochemical immunosensors,^[43,44] the proposed assay showed a lower detection limit. The high sensitivity could be attributed to the following reasons: The porous CaCO_3 sphere provided an efficient host for multiple $\text{AuNCs}/\text{HRP-Ab}_2$ loading, which greatly enhanced the detection signal. In addition, the PNCN-modified GCE was an effective matrix to immobilize biomolecules with high stability and bioactivity.

Specificity and stability of the immunosensor: The selectivity of the immunoassay was evaluated by using possible interfering substances such as immunoglobulin G (IgG) and α -fetoprotein (AFP) at a concentration of 0.1 ng mL^{-1} . The fluorescence responses for IgG and AFP were 5.8 and 7.1 % that of NSE, respectively. The DPV signals for IgG and AFP were 6.2 and 7.4 % that of NSE, respectively. This indicates that the proposed sensor has sufficient selectivity for NSE detection, and is capable of distinguishing NSE from its analogues in complex samples. The reproducibility of the immunoassay was estimated by assaying one NSE level for five replicate measurements with relative standard deviations (RSD) of 6.5%. The storage stability of $\text{CaCO}_3/\text{AuNCs}/\text{HRP-Ab}_2$ was also investigated by comparing the signals after a sandwiched immunoreaction. When the $\text{CaCO}_3/\text{AuNCs}/\text{HRP-Ab}_2$ bioconjugates were stored in PBS at 4°C, the signals remained at about 93.4% for fluorescence response and 94.6% for DPV signal after one month. This indicates that $\text{CaCO}_3/\text{AuNCs}/\text{HRP-Ab}_2$ has good storage stability at 4°C.

Application of the immunosensor in human serum: The feasibility of the immunoassay in clinical applications was investigated by analyzing several real samples, in comparison with the ELISA method. Figure 7 shows the correlation between the results obtained by fluorescence immunoassay, electrochemical immunoassay, and the ELISA method. The relative deviations between fluorescence immunoassay and ELISA method were in the range from -4.4 to +6.8%, and the relative deviation between electrochemical assay and ELISA method was 3.2–7.2%. Since there are no significant differences among the results of the three methods, the developed immunoassay may provide an interesting alternative tool for detection of proteins in clinical laboratories.

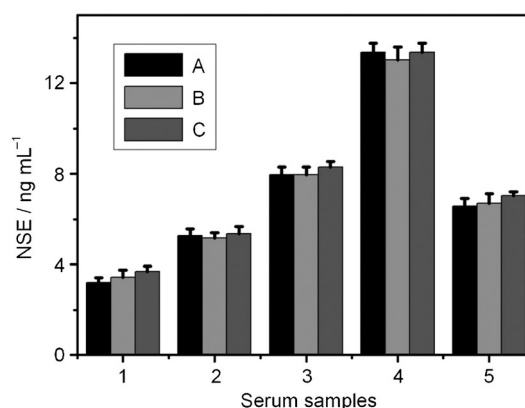


Figure 7. Comparison of serum NSE levels determined by A) fluorescence assay, B) ELISA, and C) electrochemical assay.

Conclusion

Porous CaCO_3 spheres were used for loading of AuNCs to fabricate $\text{CaCO}_3/\text{AuNCs}$ hybrid. The vaterite polymorph of CaCO_3 can be well stabilized by AuNCs. The hybrid spheres have the advantages such as porous structure, high porosity, biocompatibility, degradability, and fluorescence property and can be used as templates for the encapsulation of HRP- Ab_2 to fabricate $\text{CaCO}_3/\text{AuNCs}/\text{HRP-Ab}_2$ bioconjugates. A promising and versatile immunosensor was developed for both fluorescent and electrochemical detection of NSE by using the as-prepared bioconjugates as probes. The $\text{CaCO}_3/\text{AuNCs}$ hybrid spheres are also expected to find other potential applications such as drug delivery, diagnostics, and optics.

Experimental Section

Chemicals: H_2O_2 (30% w/v solution), $\text{HAuCl}_4 \cdot 4\text{H}_2\text{O}$ and *o*-phenylenediamine (OPD) were purchased from Shanghai Chemical Reagent Co. (Shanghai, China). Human neuron specific enolase (NSE) antigen, NSE antibody coating (Ab_1 , monoclonal), and NSE antibody (Ab_2 , polyclone) labeled with HRP (HRP- Ab_2) were purchased from Shanghai Linc-Bio Science Co. Ltd. Poly(allylamine hydrochloride) (PAH, $M=15000$), polyethylenimine (PEI), bovine serum albumin (BSA), glutaraldehyde (GLU), and Tween-20 were obtained from Aldrich Chemical Co. All other chemicals were of analytical grade. Doubly distilled water was used throughout the experiments.

Synthesis of $\text{CaCO}_3/\text{AuNCs}$ hybrid spheres: AuNCs were synthesized according to the literature (see Supporting Information for experimental details).^[19] CaCO_3 spheres were synthesized by a one-pot approach.^[34] For $\text{CaCO}_3/\text{AuNCs}$ synthesis, CaCO_3 spheres were dispersed in PAH aqueous solution (2 mg mL^{-1}) and sonicated for 10 min to make the surface positively charged. Then, CaCO_3 (50 mg) was dispersed in 50 mL of AuNCs solution (pH 7.0) and sonicated for 30 min. After centrifugation, the composites were obtained. The composites were further washed with distilled water three times and dried.

Assembly of HRP- Ab_2 into the $\text{CaCO}_3/\text{AuNCs}$ spheres: 10 mg of $\text{CaCO}_3/\text{AuNCs}$ was dispersed in a solution of HRP- Ab_2 (0.4 mg mL^{-1}) and shaken for 1 h at 4°C for enzyme absorption. The bioconjugates were then centrifuged and washed with distilled water three times. Then, the $\text{CaCO}_3/\text{AuNCs}/\text{HRP-Ab}_2$ was dispersed in PBS.

PEI-functionalized nitrogen-doped carbon nanotube (PNCN) surface for immobilization of Ab₁: Nitrogen-doped multiwalled carbon nanotubes with a nitrogen content of 3.2% were prepared as described in ref. [45]. Oxidized NCNs were prepared according our previous method.^[40] The oxidized NCNs were dispersed in a solution of PEI (2 mg mL⁻¹) and sonicated for 10 min. The final PNCNs were washed and redispersed in water to a concentration of 5.0 mg mL⁻¹. A glassy carbon electrode (GCE) was successively polished to a mirror by using 0.3 and 0.05 μm alumina slurry followed by rinsing thoroughly with water. After successive sonication in 1:1 nitric acid/water, acetone, and doubly distilled water, the electrode was rinsed with doubly distilled water and allowed to dry at room temperature. As shown schematically in Scheme 1, 5 μL of 5.0 mg mL⁻¹ PNCNs solution was first dropped onto the pretreated GCE and dried, and then immersed in a 500 μL GLU solution for 30 min. After rinsing with water, the electrode was immersed in a solution of Ab₁ for 1 h for immobilization. The immunosensor obtained was stored at 4°C when not in use.

Immunoassay procedure: GCE/PNCNs/Ab₁ was blocked with 100 μL of 10 mM BSA for 30 min at room temperature and washed with PBST. After incubation with 60 μL of NSE for 30 min at 37°C, the electrode was incubated in 60 μL of diluted CaCO₃/AuNCs/HRP-Ab₂ solution for 30 min. Finally, the electrode was washed with PBS to remove unspecifically bound conjugates. The fluorescence immunoassays were performed on a fluorescence microscope. The electrochemical immunoassay measurements were performed on a CHI 660 electrochemical analyzer (CHI Co., USA) with a conventional three-electrode system comprised of platinum wire as the auxiliary electrode, a saturated calomel electrode (SCE) as the reference, and a modified GCE as the working electrode. The immunosensor was then placed in an electrochemical cell that contained 3.0 mL of PBS, 2.0 mM *o*-phenylenediamine (OPD) and 4.0 mM H₂O₂, which was deoxygenized with nitrogen for 5 min and maintained under a nitrogen atmosphere at room temperature. The differential pulse voltammetric measurements were performed from -0.3 to -0.8 V with a pulse amplitude of 50 mV and a pulse width of 50 ms.

Apparatus and characterizations: The morphologies of materials were observed by TEM (JEOL JEM-200CX) and SEM (LEO153VP). BET data were collected with a Micromeritics ASAP 2020 surface area and porosity analyzer at 77 K. The BET surface area was calculated from the linear part of the BET plot. The pore-size distribution plots were obtained by using the Barrett–Joyner–Halenda (BJH) model. Confocal micrographs were taken with a Leica TCS-SL confocal scanning system mounted to a Leica Aristoplan and equipped with a 40× oil-immersion objective with a numerical aperture of 1.25. The fluorescence spectra were recorded on a RF-5301 PC spectrofluorophotometer (SHIMADZU). Electrochemical experiments were performed with a CHI660 workstation (Shanghai Chenhua, Shanghai, China). All of the differential pulse voltammetric measurements were carried out by using a conventional three-electrode system with a glassy carbon working electrode, SCE, and a platinum counterelectrode.

Acknowledgements

We greatly appreciate the support of the National Natural Science Foundation of China (No: 21075061, 21103088, 21121091) and the Natural Science Foundation of Jiangsu Province (BK2010363). This work is also supported by National Basic Research Program of China (2011CB933502).

- [1] T. Huang, R. W. Murray, *J. Phys. Chem. B* **2001**, *105*, 12498–12502.
- [2] J. H. Chen, A. A. Mohamed, H. E. Abdou, J. A. K. Bauer, J. P. Fackler, A. E. Bruce, M. R. M. Bruce, *Chem. Commun.* **2005**, 1575–1577.
- [3] B. S. Gonzalez, M. J. Rodriguez, C. Blanco, J. Rivas, M. A. Lopez-Quintela, J. M. G. Martinho, *Nano Lett.* **2010**, *10*, 4217–4221.
- [4] M. A. H. Muhammed, P. K. Verma, S. K. Pal, A. Retnakumari, M. Koyakutty, S. Nair, T. Pradeep, *Chem. Eur. J.* **2010**, *16*, 10103–10112.

- [5] I. L. Garzon, M. R. Beltran, G. Gonzalez, I. Gutierrez-Gonzalez, K. Michaelian, J. A. Reyes-Nava, J. I. Rodriguez-Hernandez, *Eur. Phys. J. D* **2003**, *24*, 105–109.
- [6] A. Lechtken, D. Schooss, J. R. Stairs, M. N. Blom, F. Furche, N. Morgner, O. Kostko, B. von Issendorff, M. M. Kappes, *Angew. Chem.* **2007**, *119*, 3002–3006; *Angew. Chem. Int. Ed.* **2007**, *46*, 2944–2948.
- [7] X. Lopez-Lozano, L. A. Perez, I. L. Garzon, *Phys. Rev. Lett.* **2006**, *97*.
- [8] M. A. Munoz-Marquez, E. Guerrero, A. Fernandez, P. Crespo, A. Hernando, R. Lucena, J. C. Conesa, *J. Nanopart. Res.* **2010**, *12*, 1307–1318.
- [9] J. F. Hicks, A. C. Templeton, S. W. Chen, K. M. Sheran, R. Jasti, R. W. Murray, J. Debord, T. G. Schaaf, R. L. Whetten, *Anal. Chem.* **1999**, *71*, 3703–3711.
- [10] D. T. Miles, R. W. Murray, *Anal. Chem.* **2003**, *75*, 1251–1257.
- [11] T. H. Lee, J. I. Gonzalez, J. Zheng, R. M. Dickson, *Acc. Chem. Res.* **2005**, *38*, 534–541.
- [12] J. R. Aranzaes, C. Belin, D. Astruc, *Chem. Commun.* **2007**, 3456–3458.
- [13] H. Wei, Z. D. Wang, L. M. Yang, S. L. Tian, C. J. Hou, Y. Lu, *Analyst* **2010**, *135*, 1406–1410.
- [14] D. H. Hu, Z. H. Sheng, P. F. Zhang, L. T. Cai, *Analyst* **2010**, *135*, 1411–1416.
- [15] Y. L. Liu, K. L. Ai, X. L. Cheng, L. H. Huo, L. H. Lu, *Adv. Funct. Mater.* **2010**, *20*, 951–956.
- [16] R. C. Triulzi, M. Micic, S. Giordani, M. Serry, W. A. Chiou, R. M. Leblanc, *Chem. Commun.* **2006**, 5068–5070.
- [17] C. C. Huang, C. K. Chiang, Z. H. Lin, K. H. Lee, H. T. Chang, *Anal. Chem.* **2008**, *80*, 1497–1504.
- [18] M. J. Wang, C. Y. Sun, L. Y. Wang, X. H. Ji, Y. B. Bai, T. J. Li, J. H. Li, *J. Pharm. Biomed. Anal.* **2003**, *33*, 1117–1125.
- [19] J. Xie, Y. Zheng, J. Y. Ying, *J. Am. Chem. Soc.* **2009**, *131*, 888–889.
- [20] D. V. Volodkin, N. I. Larionova, G. B. Sukhorukov, *Biomacromolecules* **2004**, *5*, 1962–1972.
- [21] W. Y. Cai, L. D. Feng, S. H. Liu, J. J. Zhu, *Adv. Funct. Mater.* **2008**, *18*, 3127–3136.
- [22] C. Y. Wang, C. Y. He, Z. Tong, X. X. Liu, B. Y. Ren, F. Zeng, *Int. J. Pharm.* **2006**, *308*, 160–167.
- [23] W. Y. Cai, Q. Xu, X. N. Zhao, J. H. Zhu, H. Y. Chen, *Chem. Mater.* **2006**, *18*, 279–284.
- [24] D. Shan, S. X. Wang, H. G. Xue, S. Cosnier, *Electrochem. Commun.* **2007**, *9*, 529–534.
- [25] W. Sun, R. F. Gao, K. Jiao, *Electroanalysis* **2007**, *19*, 1368–1374.
- [26] X. H. Guo, S. H. Yu, G. B. Cai, *Angew. Chem.* **2006**, *118*, 4081–4085; *Angew. Chem. Int. Ed.* **2006**, *45*, 3977–3981.
- [27] Y. Deng, Y. Cai, Z. Sun, J. Liu, C. Liu, J. Wei, W. Li, C. Liu, Y. Wang, D. Zhao, *J. Am. Chem. Soc.* **2010**, *132*, 8466–8473.
- [28] B.-H. Jun, M. S. Noh, J. Kim, G. Kim, H. Kang, M.-S. Kim, Y.-T. Seo, J. Baek, J.-H. Kim, J. Park, S. Kim, Y.-K. Kim, T. Hyeon, M.-H. Cho, D. H. Jeong, Y.-S. Lee, *Small* **2010**, *6*, 119–125.
- [29] H. Zhou, J. Chen, E. Sutter, M. Feygensohn, M. C. Aronson, S. S. Wong, *Small* **2010**, *6*, 412–420.
- [30] Y. Zhu, J. Shen, K. Zhou, C. Chen, X. Yang, C. Li, *J. Phys. Chem. C* **2011**, *115*, 1614–1619.
- [31] B. S. Munge, A. L. Coffey, J. M. Doucette, B. K. Somba, R. Malhotra, V. Patel, J. S. Gutkind, J. F. Rusling, *Angew. Chem.* **2011**, *123*, 8061–8064; *Angew. Chem. Int. Ed.* **2011**, *50*, 7915–7918.
- [32] L. Yuan, X. Hua, Y. Wu, X. Pan, S. Liu, *Anal. Chem.* **2011**, *83*, 6800–6809.
- [33] P. Martens, A. Raabe, P. Johnsson, *Stroke* **1998**, *29*, 2363–2366.
- [34] W. Wei, G. H. Ma, G. Hu, D. Yu, T. McLeish, Z. G. Su, Z. Y. Shen, *J. Am. Chem. Soc.* **2008**, *130*, 15808–15810.
- [35] M. Fujiwara, K. Shiokawa, K. Morigaki, Y. C. Zhu, Y. Nakahara, *Chem. Eng. J.* **2008**, *137*, 14–22.
- [36] Y. J. Huang, D. Li, J. H. Li, *Chem. Phys. Lett.* **2004**, *389*, 14–18.
- [37] J. H. Li, S. J. Dong, *J. Electroanal. Chem.* **1997**, *431*, 19–22.
- [38] N. Nassrallah-Aboukais, A. Boughriet, J. Laureyns, L. Gengembre, A. Aboukais, *Chem. Mater.* **1999**, *11*, 44–51.

- [39] E. E. Ferapontova, *Electroanalysis* **2004**, *16*, 1101–1112.
- [40] J.-J. Zhang, F.-F. Cheng, T.-T. Zheng, J.-J. Zhu, *Anal. Chem.* **2010**, *82*, 3547–3555.
- [41] R. Cui, H. Huang, Z. Yin, D. Gao, J.-J. Zhu, *Biosens. Bioelectron.* **2008**, *23*, 1666–1673.
- [42] J. G. Stonehuerner, J. Zhao, J. P. Odaly, A. L. Crumbliss, R. W. Henkens, *Biosens. Bioelectron.* **1992**, *7*, 421–428.
- [43] Z. Zhong, N. Peng, Y. Qing, J. Shan, M. Li, W. Guan, N. Dai, X. Gu, D. Wang, *Electrochim. Acta* **2011**, *56*, 5624–5629.
- [44] A. C. Barton, F. Davis, S. P. J. Higson, *Anal. Chem.* **2008**, *80*, 9411–9416.
- [45] H. Chen, Y. Yang, Z. Hu, K. Huo, Y. Ma, Y. Chen, X. Wang, Y. Lu, *J. Phys. Chem. B* **2006**, *110*, 16422–16427.

Received: September 14, 2011

Revised: December 31, 2011

Published online: March 15, 2012